

## Transparent flexible organic thin-film transistors that use printed single-walled carbon nanotube electrodes

Qing Cao, Zheng-Tao Zhu, Maxime G. Lemaitre, Ming-Gang Xia, Moonsub Shim, and John A. Rogers<sup>a)</sup>

Department of Chemistry, Beckman Institute and Frederick Seitz Materials Research Laboratory, University of Illinois at Urbana-Champaign, Urbana, Illinois 61801

(Received 29 October 2005; accepted 17 January 2006; published online 15 March 2006)

Electrodes based on printed networks of single-walled carbon nanotubes (SWNTs) are integrated with ultrathin layers of the organic semiconductor pentacene to produce bendable, transparent thin-film transistors on plastic substrates. The physical and structural properties of the SWNTs lead to the remarkably good electrical contacts with the pentacene. Optical transmittances of  $\sim 70\%$ , device mobilities  $>0.5 \text{ cm}^2 \text{ V}^{-1} \text{ s}^{-1}$ , ON/OFF ratios  $>10^5$  and tensile strains as large as 1.8% are achieved in devices of this type. These characteristics indicate promise for applications in power conserving flexible display systems and other devices. © 2006 American Institute of Physics.

[DOI: 10.1063/1.2181190]

Thin-film transistors (TFTs) based on transparent electronic materials, such as conductive oxides<sup>1</sup> and single-walled carbon nanotubes (SWNTs),<sup>2,3</sup> could be useful for unusual applications such as see-through active matrix displays or certain classes of secure electronics. These devices could also be attractive as replacements for amorphous or polycrystalline silicon TFTs in backlit active-matrix liquid crystal displays due to their ability to provide high effective aperture ratios. TFTs based on organic semiconducting materials have potential applications in this area and in related systems that use flexible substrates. The ability to pattern these materials using printing-like processes over large areas on low temperature plastics is an important feature.<sup>4-6</sup> In addition, because many organic semiconductors are weakly absorbing in the visible (compared to, for example, *a*-Si), they can be useful in transparent systems. Recent work demonstrates transparent thin-film transistors (TTFTs) that use electrodes of indium tin oxide (ITO) and  $\text{NiO}_x$  with organic semiconductors such as phthalocyanine and pentacene.<sup>7,8</sup> The electrical performance (mobility  $\sim 5 \times 10^{-3} \text{ cm}^2 \text{ V}^{-1} \text{ s}^{-1}$ ) and degree of optical transparency (25%–30%) in these devices are, however, worse than those that have been obtained with the inorganic oxides. A significant challenge is that the contacts between transparent inorganic conductors and organic semiconductors are often poor and characterized by large Schottky barriers (SBs). We report here a class of mechanically flexible organic TTFTs based on ultrathin films of pentacene and transparent electrodes of networks of SWNTs formed by transfer printing of pristine tube grown by chemical vapor deposition (CVD). The excellent optical, electrical and mechanical properties of the devices and the remarkably good contacts that form between the pentacene and the SWNT electrodes represent potentially important results.

Figure 1(a) shows a schematic illustration of this type of organic TTFT. To build these devices, a sheet of poly(ethylene terephthalate) (PET; thickness  $\sim 180 \mu\text{m}$ ) was first spin coated with a layer (thickness 580 nm) of epoxy (3000 rpm

for 30 s of Microchem SU8-5 diluted with 66% of SU8-2000 thinner). Transfer printing<sup>9</sup> a CVD SWNT network<sup>10</sup> with moderately high coverage ( $\sim 55 \text{ tubes}/\mu\text{m}^2$ ) and low sheet resistance ( $9.5 \pm 0.1 \text{ k}\Omega/\text{sq}$ ), onto the epoxy formed the gate electrode. A uniform  $\text{AlO}_x$  film (thickness 100 nm) deposited on top of the gate by electron beam evaporation ( $3 \times 10^{-6}$  Torr; Temescal BJD1800) and exposed to a brief oxygen reactive ion etching step (RIE; Plasmatherm RIE system, 20 sccm  $\text{O}_2$  flow with a chamber base pressure of

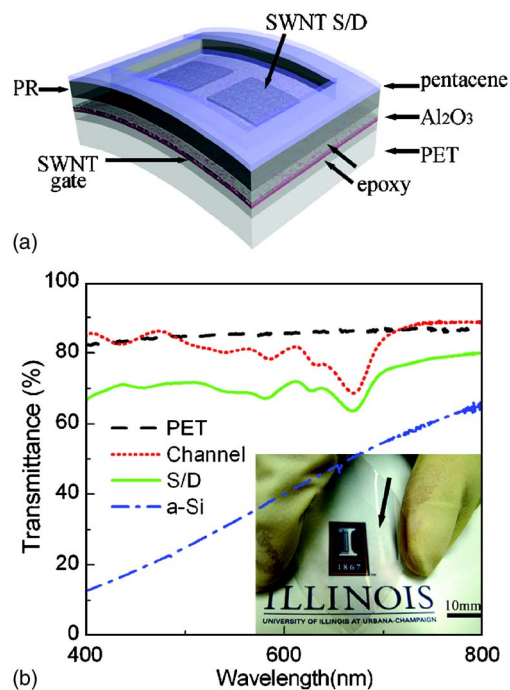


FIG. 1. (Color online) (a) Schematic geometry of an organic TTFT on a plastic substrate (PET). Transfer printed SWNT films form the source/drain and gate electrodes. (b) Optical transmission spectra for the PET substrate, 15 nm amorphous Si (*a*-Si) on PET and the device structure measured through the source/drain regions and the channel regions. Inset: Optical image of an array of such devices, positioned above some printed text on paper to illustrate the degree of optical transparency. The arrow indicates the source/drain structures, which appear as faint gray squares.

<sup>a)</sup> Author to whom correspondence should be addressed; electronic mail: jrogers@uiuc.edu

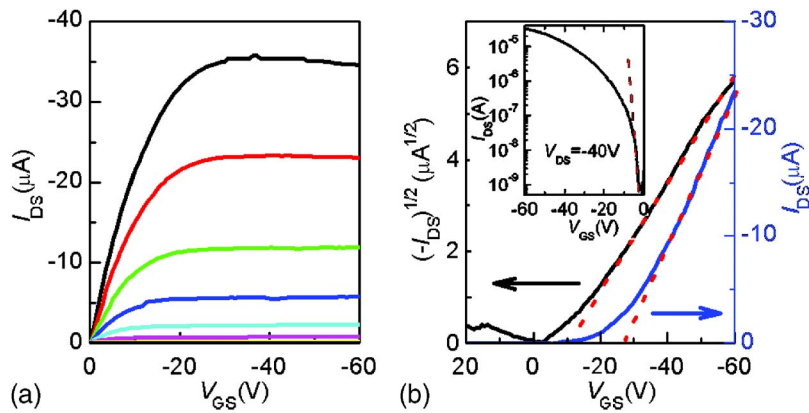


FIG. 2. (Color online) (a) Current-voltage characteristics of an optimized organic TFT that uses SWNT electrodes. The channel width is  $750 \mu\text{m}$ , the channel length is  $30 \mu\text{m}$ . The gate voltage varies between 0 and  $-60 \text{ V}$  in steps of  $-10 \text{ V}$ . (b) Transfer curve (right axis) in the triode region ( $V_{\text{DS}} = -10 \text{ V}$ ) and  $\sqrt{|I_{\text{DS}}|}$  vs  $V_{\text{GS}}$  curve (left axis) in the saturation region ( $V_{\text{DS}} = -40 \text{ V}$ ) of the same device. The dashed lines indicate the slopes used to determine the linear and saturation mobilities. Inset: Logarithm plot of the transfer curve in the saturation region ( $V_{\text{DS}} = -40 \text{ V}$ ). The dashed line indicates the slope used for determining the subthreshold swing.

100 mTorr, 100 W rf power for 30 s) promotes the wetting of another spin cast layer of epoxy (thickness  $580 \text{ nm}$ ). The  $\text{Al}_2\text{O}_3/\text{epoxy}$  bilayer (capacitance  $4.8 \text{ nF/cm}^2$ , as measured with a capacitance meter, Agilent 4288A), formed the gate dielectric. A film of SWNTs with high coverage ( $>200 \text{ tubes}/\mu\text{m}^2$ , thickness  $20\text{--}30 \text{ nm}$ ) and low sheet resistance ( $265 \pm 2 \Omega/\text{sq}$ ) patterned by oxygen RIE (Plasmatherm RIE system,  $20 \text{ sccm O}_2$  flow with a chamber base pressure of 100 mTorr, 100 W rf power for 240 s) through a photoresist mask (defined by standard photolithography with AZ5214 photoresist) on the growth substrate (Si wafer with  $100 \text{ nm SiO}_2$ ) defined source and drain electrode structures. The same printing method used for the gate transferred these SWNT electrodes onto the epoxy/ $\text{Al}_2\text{O}_3$ /SWNT/epoxy/PET substrate. The final step of the fabrication involved patterning a layer of photoresist (AZ 5214, thickness  $1.4 \mu\text{m}$ ) on the substrate and then thermally evaporating (base pressure  $3 \times 10^{-6} \text{ Torr}$ ,  $0.5 \text{ \AA/s}$  at room temperature) a  $15\text{-nm}$ -thick layer of pentacene (Aldrich, 99% purity). The relief structure associated with the resist electrically isolated the devices. The thickness of pentacene layer was chosen to slightly exceed the thickness of the transport layer.<sup>11</sup> The density of the SWNT networks was chosen to balance optical transparency with low sheet resistance properties. We found that the electrical performance of the devices could be improved significantly by treating the top surface of the epoxy with octadecyltrichlorosilane (OTS; 1 mM solution of OTS in toluene for 12 h at 300 K) prior to the pentacene deposition, as has been described in the literature for the case of  $\text{SiO}_2$  dielectrics.<sup>12</sup> We speculate that some of the OTS adsorbs to the surface of the epoxy, thereby changing, in a favorable way, the wetting characteristics to the pentacene.

Figure 1(b) presents the optical transmittance for wavelengths between 400 and 800 nm (Agilent 8453 spectrometer). The average transmittances through the channel region and source/drain region (including all layers and the PET substrate) are  $\sim 80\%$  and  $\sim 70\%$  respectively, which is much better than amorphous Si with the same thickness and comparable to TFTs built with inorganic conductive oxides.<sup>1,13</sup> The absorption peaks at 668 and 628 nm correspond with the Davydov splitting of the highest occupied molecular orbital-lowest unoccupied molecular orbital gap of pentacene.<sup>14</sup> The peaks at 582 and 542 nm correspond with the Frenkel exciton and second lowest unoccupied molecular orbital of pentacene, respectively.<sup>15</sup> The SWNT electrodes do not contribute significantly to variations in the transmittance in this wavelength range. The inset shows an image of an array of these TFTs positioned above a logo of University of Illinois

at Urbana-Champaign to illustrate the level of optical transparency. The source/drain structures appear as faint gray areas indicated by the arrow.

Figure 2 presents the performance of an OTS treated device that exhibits a mobility of  $\sim 0.6 \text{ cm}^2 \text{ V}^{-1} \text{ s}^{-1}$ , an ON/OFF ratio of  $10^5$  and a subthreshold swing of  $\sim 1.4 \text{ V/dec}$ . Studies of collections of devices similar to this one, but without the OTS layer, show good scaling properties: saturation and linear mobilities are comparable to one another and independent of channel length. These results suggest good contact characteristics between the SWNT electrodes and the pentacene.

To gain a better understanding of the SWNT/pentacene contacts, we fabricated control devices that have the same layout as the organic SWNT TFTs but which use  $30\text{-nm}$ -thick Au source/drain electrodes (electron beam evaporated, Temescal BJD1800,  $2 \times 10^{-6} \text{ Torr}$ ) instead of SWNTs. The pentacene layers for both organic TFTs and Au controls were deposited in the same run. Figure 3(b) and 3(d) show the resistances of devices measured in ON state ( $R_{\text{ON}}$ ) in the linear region, and multiplied by  $W$ , as a function

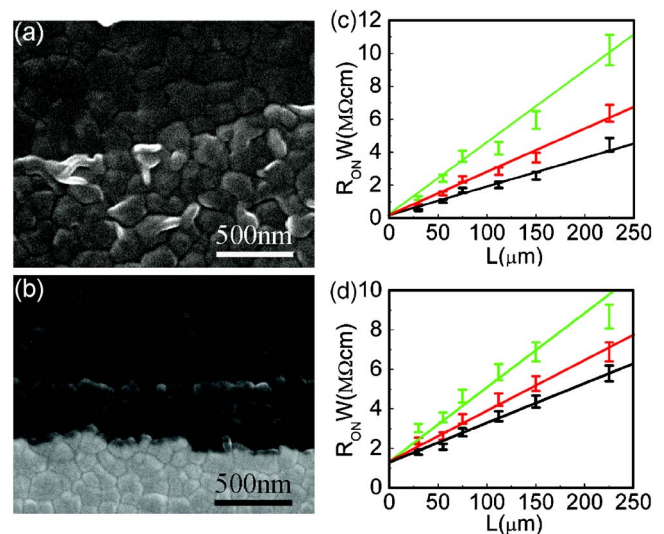


FIG. 3. (Color online) (a) Scanning electron microscope image of the interface between SWNT electrode and the channel region. The SWNT electrode is on the bottom side of the picture. (b) Width normalized device resistance of organic TFTs with SWNT electrodes as a function of channel length at gate voltages from  $-40$  to  $-60 \text{ V}$ . (c) scanning electron microscope image of the interface between Au electrode and the channel region. The Au electrode is on the bottom side of the picture. (d) Width normalized device resistance of organic TFTs with Au electrodes as a function of channel length at gate voltages from  $-40$  to  $-60 \text{ V}$ .

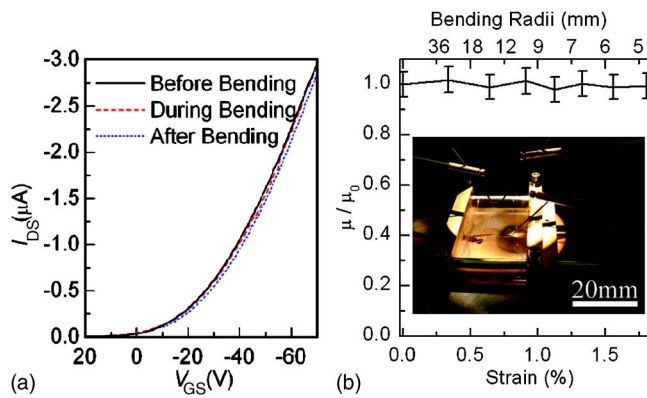


FIG. 4. (a) Transfer curves of a device before bending, during bending to a radius of 5 mm (i.e., tensile strain of 1.8%) and after relaxing. (b) Variation of normalized device mobility ( $\mu/\mu_0$ ) with tension strain. Inset: Bending test of a flexible organic TFT with SWNT electrodes.

of  $L$  at different gate voltages for SWNT and Au devices, respectively. In this regime,  $R_{ON}$  can be approximated as the sum of an  $L$  dependent channel resistance and an  $L$  independent parasitic resistance ( $R_C$ ) at the contact.<sup>16</sup> As determined from the intercept of linear fitting, the parasitic resistance,  $R_C$ , is significantly smaller in the SWNT compared to the Au devices. Also, the Au devices show a strongly nonohmic response in the triode region, consistent with previous reports.<sup>17</sup>

The good contacts in the SWNT case are consistent with other observations<sup>18,19</sup> and can be attributed to the structure and physical properties of the SWNTs. First, because both the pentacene and SWNT molecule share the same conjugated carbon hexagonal ring structure, the pentacene molecules, when deposited onto SWNT electrodes, stack on the surface of SWNT in a commensurate configuration, possibly similar to the epitaxial growth observed on graphite due to favorable  $\pi$ - $\pi$  interactions. This growth can lead to interfaces that facilitate the electron injection from SWNT.<sup>20</sup> Scanning electron microscope images (Hitachi S-4700) of the SWNT-pentacene [Fig. 3(a)] and Au-pentacene [Fig. 3(c)] interfaces, show no disruption in pentacene grain structure near the SWNT electrodes but significantly smaller grain sizes near the Au. This latter behavior leads to a large number of grain boundaries that can lead to poor injection and transport near the contacts.<sup>21</sup> Second, the high aspect ratio of the SWNT leads to field focusing that can depress the SB.<sup>19,22</sup> Third, compared with metals, SWNTs do not have a strong surface electronic component. As a result, the surface dipole barrier of SWNT electrodes is much lower compared with their Au counterpart, which enables more effective carrier injection.<sup>23</sup>

In addition to the good optical, electrical and contact properties, the SWNT based pentacene TTFTs have excellent mechanical flexibility, in part due to the robust bending properties of SWNTs and SWNT networks.<sup>24</sup> Figure 4 shows some results of bending tests, using systems described previously.<sup>25</sup> Figure 4(a) compares the performance of a transistor before, during and after bending to a radius of 5 mm (i.e., tensile strain of 1.8%). Tensile strains greater than 1.5%–2% lead to failure of dielectric layer, as evidenced by large gate leakage currents. Figure 4(b) shows the mobility ( $\mu$ ) in the saturation region normalized by the value without strain ( $\mu_0$ ), as a function of bending induced tensile strain.

Unlike observations in devices with Au electrodes,<sup>26</sup> there is no significant change in mobility during bending, which may be due to the combined effects of good contacts and mechanical properties of the SWNT electrodes.

In summary, this letter demonstrates the integration of transparent SWNT electrodes with organic semiconductors to form flexible TTFTs on plastic substrates. These devices show good electrical properties (negligible contact resistances, and mobilities larger than  $0.5 \text{ cm}^2 \text{ V}^{-1} \text{ s}^{-1}$ ), bendability (radii of curvature  $<5 \text{ mm}$ ) and optical transparency ( $\sim 70\%$ ). These features, combined with the printability of the active materials, suggest a possible role for devices of this type in transparent and other future electronic systems.

This work was supported by DARPA-funded AFRL-managed Macroelectronics Program Contract No. FA8650-04-C-7101, the U. S. Department of Energy under Grant No. DEFG02-91-ER45439 and the NSF through Grant No. NIRT-0403489. M.-G.X. thanks Xian Jiaotong University for financial support.

- <sup>1</sup>R. L. Hoffman, B. J. Norris, and J. F. Wager, Appl. Phys. Lett. **82**, 733 (2003).
- <sup>2</sup>E. Artukovic, M. Kaempgen, D. Hecht, S. Roth, and G. Gruner, Nano Lett. **5**, 757 (2005).
- <sup>3</sup>Q. Cao, S.-H. Hur, Z.-T. Zhu, Y. Sun, C. Wang, M. Meitl, M. Shim, and J. A. Rogers, Adv. Mater. (Weinheim, Ger.) **18**, 304 (2006).
- <sup>4</sup>J. A. Rogers, Z. Bao, K. Baldwin, A. Dodabalapur, B. Crone, V. R. Raju, V. Kuck, H. Katz, K. Amundson, J. Ewing, and P. Drzaic, Proc. Natl. Acad. Sci. U.S.A. **98**, 4835 (2001).
- <sup>5</sup>H. E. A. Huitema, G. H. Gelinck, J. van der Putten, K. E. Kuijk, C. M. Hart, E. Cantatore, P. T. Herwig, A. van Breemen, and D. M. de Leeuw, Nature (London) **414**, 599 (2001).
- <sup>6</sup>K. Nomoto, N. Hirai, N. Yoneya, N. Kawashima, M. Noda, M. Wada, and J. Kasahara, IEEE Trans. Electron Devices **52**, 1519 (2005).
- <sup>7</sup>H. Ohta, T. Kambayashi, K. Nomura, M. Hirano, K. Ishikawa, H. Takezoe, and H. Hosono, Adv. Mater. (Weinheim, Ger.) **16**, 312 (2004).
- <sup>8</sup>J. Lee, D. K. Hwang, J.-M. Choi, K. Lee, J. H. Kim, S. Im, J. H. Park, and E. Kim, Appl. Phys. Lett. **87**, 023504 (2005).
- <sup>9</sup>S.-H. Hur, O. O. Park, and J. A. Rogers, Appl. Phys. Lett. **86**, 243502 (2005).
- <sup>10</sup>G. Y. Zhang, D. Mann, L. Zhang, A. Javey, Y. M. Li, E. Yenilmez, Q. Wang, J. P. McVittie, Y. Nishi, J. Gibbons, H. J. Dai, Proc. Natl. Acad. Sci. U.S.A. **102**, 16141 (2005).
- <sup>11</sup>R. Ruiz, A. Papadimitratos, A. C. Mayer, and G. G. Malliaras, Adv. Mater. (Weinheim, Ger.) **17**, 1795 (2005).
- <sup>12</sup>M. Shtein, J. Mapel, J. B. Benziger, and S. R. Forrest, Appl. Phys. Lett. **81**, 268 (2002).
- <sup>13</sup>E. Fortunato, P. Barquinha, A. Pimentel, A. Goncalves, A. Marques, L. Pereira, and R. Martins, Adv. Mater. (Weinheim, Ger.) **17**, 590 (2005).
- <sup>14</sup>T. Minakata, I. Nagoya, and M. Ozaki, J. Appl. Phys. **69**, 7354 (1991).
- <sup>15</sup>J. Lee, S. S. Kim, K. Kim, J. H. Kim, and S. Im, Appl. Phys. Lett. **84**, 1701 (2004).
- <sup>16</sup>S. Luan and G. W. Neudeck, J. Appl. Phys. **72**, 766 (1992).
- <sup>17</sup>C. D. Dimitrakopoulos and D. J. Maseo, IBM J. Res. Dev. **45**, 11 (2001).
- <sup>18</sup>M. Lefenfeld, G. Blanchet, and J. A. Rogers, Adv. Mater. (Weinheim, Ger.) **15**, 1188 (2003).
- <sup>19</sup>P. F. Qi, A. Javey, M. Rolandi, Q. Wang, E. Yenilmez, and H. J. Dai, J. Am. Chem. Soc. **126**, 11774 (2004).
- <sup>20</sup>K. Tsukagoshi, I. Yagi, and Y. Aoyagi, Appl. Phys. Lett. **85**, 1021 (2004).
- <sup>21</sup>I. Kymissis, C. D. Dimitrakopoulos, and S. Purushothaman, IEEE Trans. Electron Devices **48**, 1060 (2001).
- <sup>22</sup>S. Heinze, J. Tersoff, R. Martel, V. Derycke, J. Appenzeller, and P. Avouris, Phys. Rev. Lett. **89**, 106801 (2002).
- <sup>23</sup>N. Koch, J. Ghijssen, A. Elschner, R. L. Johnson, J.-J. Pireaux, J. Schwartz, and A. Kahn, Appl. Phys. Lett. **82**, 70 (2003).
- <sup>24</sup>B. Yakobson and P. Avouris, Top. Appl. Phys. **80**, 287 (2001).
- <sup>25</sup>E. Menard, R. G. Nuzzo, and J. A. Rogers, Appl. Phys. Lett. **86**, 093507 (2005).
- <sup>26</sup>T. Sekitani, Y. Kato, S. Iba, H. Shinaoka, and T. Someya, Appl. Phys. Lett. **86**, 073511 (2005).